ADVANCED FUNCTIONAL MATERIALS
www.afm-journal.de

Engineering of the Electron Transport Layer/Perovskite Interface in Solar Cells Designed on TiO_2 Rutile Nanorods

Fahimeh Shahvaranfard, Marco Altomare, Yi Hou, Seyedsina Hejazi, Wei Meng, Benedict Osuagwu, Ning Li, Christoph J. Brabec, and Patrik Schmuki**

The engineering of the electron transport layer (ETL)/light absorber interface is explored in perovskite solar cells. Single-crystalline TiO_2 nanorod (NR) arrays are used as ETL and methylammonium lead iodide (MAPI) as light absorber. A dual ETL surface modification is investigated, namely by a $TiCl_4$ treatment combined with a subsequent $PC_{61}BM$ monolayer deposition, and the effects on the device photovoltaic performance were evaluated with respect to single modifications. Under optimized conditions, for the combined treatment synergistic effects are observed that lead to remarkable enhancements in cell efficiency, from 14.2% to 19.5%, and to suppression of hysteresis. The devices show J_{SC}, V_{OC}, and fill factor as high as 23.2 mA cm^{-2}, 1.1 V, and 77%, respectively. These results are ascribed to a more efficient charge transfer across the ETL/perovskite interface, which originates from the passivation of defects and trap states at the ETL surface. To the best of our knowledge, this is the highest cell performance ever reported for TiO_2 NR-based solar cells fabricated with conventional MAPI light absorber. Perspective wise, this ETL surface functionalization approach combined with more recently developed and better performing light absorbers, such as mixed cation/anion hybrid perovskite materials, is expected to provide further performance enhancements.

1. Introduction

In the past few years, organic–inorganic hybrid halide perovskite materials have come into focus due to their unique optoelectronic properties such as strong visible light absorbance and high carrier mobility.[1–5] The implementation of this class of materials into solar cells has led to a new generation of rapidly developing photovoltaic technologies. Cell efficiencies have reached beyond 25% in a short period of time, making perovskite solar cells (PSCs) one of the fast-advancing solar technology to date.[6,7]

PSCs are mainly classified into three types of architectures depending on the morphology of the beneath interface layer, e.g. planar, mesoporous, or nanostructured.[8–10] In all configurations, both the electron transport layer (ETL), typically a TiO_2 or SnO_2 scaffold, and its interface with the perovskite light absorber play a crucial role for the overall cell performance.[11]

1D TiO_2 nanomaterials such as nanorods (NRs), nanowires, and nanotubes have meanwhile been widely applied to the fabrication of nanostructured ETLs as they can provide advantageous features, such as improved interfacial contact with the perovskite and enhanced charge diffusion, due to their large available surface area and directional charge transport paths. Both these features can be exploited to limit the charge recombination in the perovskite and at the ETL/perovskite interface.[8,9,12–15]

Layers of TiO_2 nanotubes, produce, for example, by anodic oxidation of Ti metal or by selective core-etching of hydrothermally-grown NRs, have been explored as ETL for perovskite cells though with limited success, i.e., typical efficiency values are <15%.[15–18] A main reason for the limited performance can

F. Shahvaranfard, Dr. M. Altomare, S. Hejazi, B. Osuagwu, Prof. P. Schmuki
Institute for Surface Science and Corrosion WW4-LKO
Department of Materials Science and Engineering
University of Erlangen-Nuremberg
Martensstrasse 7, 91058 Erlangen, Germany
E-mail: marco.altomare@fau.de; schmuki@ww.uni-erlangen.de

The ORCID identification number(s) for the author(s) of this article can be found under https://doi.org/10.1002/adfm.201909738.

DOI: 10.1002/adfm.201909738

Dr. Y. Hou, W. Meng, Dr. N. Li, Prof. C. J. Brabec
Institute of Materials for Electronics and Energy Technology (i-MEET)
Department of Materials Science and Engineering
University of Erlangen-Nuremberg
Martensstrasse 7, 91058 Erlangen, Germany
Dr. N. Li, Prof. C. J. Brabec
Helmholtz Institute Erlangen-Nürnberg for Renewable Energy (HI ERN)
Immerwahrstr. 2, 91058 Erlangen, Germany
Dr. N. Li
National Engineering Research Center for Advanced Polymer Processing Technology
Zhengzhou University
450002 Zhengzhou, China
Prof. P. Schmuki
Chemistry Department
Faculty of Sciences
King Abdulaziz University
80203 Jeddah, Kingdom of Saudi Arabia

be the incomplete filling of pores with the perovskite. This can affect the light absorbance, the charge transport and interfacial transfer, and thus the overall cell efficiency.

In this context, rutile TiO_2 NRs provide better properties, i.e., an open structure for an effective infiltration of the perovskite and a single crystalline nature. The latter can, for example in contrast to anodically grown polycrystalline TiO_2 nanotubes, provide enhanced electron transfer properties[10,12] and thus, in principle, better cell performances.

Nevertheless, aside from the ETL morphology, key to the device efficiency is also to optimize the ETL/perovskite interface properties, e.g. by passivation of the TiO_2 surface defects and trap states.[4,19,20] To this end, titanium tetrachloride ($TiCl_4$) treatment, has been reported as a most efficient approach to improve TiO_2 electron transport ability: it forms at the treated surface a nm-thick layer of TiO_2 anatase nanoparticles (NPs, with size in the 5–10 nm range) that typically favors a more efficient charge extraction across the ETL/perovskite interface, thereby limiting photon losses ascribed to charge recombination in the light absorber.[3,21,22]

An alternative approach is to introduce an additive between the ETL and perovskite layer. Phenyl-C61-butyric acid methyl ester ($PC_{61}BM$), a thin organic surface modifier, was recently implemented in perovskite cells' technology as an efficient interlayer to passivate surface defects in both the metal oxide ETL and perovskite light absorber. This can substantially reduce the device hysteresis and improve the cell efficiency.[23,24]

Herein, we discuss the synergistic effects in cell performance enhancement achieved by surface modification of TiO_2 NR ETLs by $TiCl_4$ treatment combined with $PC_{61}BM$ monolayer deposition. Such an engineering of the TiO_2 ETL/perovskite interface leads to a remarkable increase of the cell efficiency up to 19.5% for our champion device (17.9% average PCE). Our results suggest that on the one hand, the $TiCl_4$ surface treatment allows for improving the surface contact of the ETL with the perovskite and thus increases the cell performance due to a more efficient charge transfer. On the other hand, the $PC_{61}BM$ monolayer, by passivating surface defects at the TiO_2 ETL/perovskite interface, enhances the efficiency even further and leads to a nearly complete suppression of the device hysteresis.

2. Results and Discussion

To optimize the PSCs, we engineered the ETL/perovskite interface using hydrothermally grown TiO_2 NRs modified by $TiCl_4$ and/or $PC_{61}BM$ treatments. The TiO_2 NR arrays were decorated with different loadings of TiO_2 anatase NPs; for this the NRs were treated in $TiCl_4$ solutions of different concentrations, i.e., 50, 100, and 200×10^{-3} M. After $TiCl_4$ treatment and annealing, the ETL were used to fabricate the PSCs as outlined in the Experimental Section. Temperature and time of the $TiCl_4$ treatment were kept constant for all the samples.

Figure 1 and Figure S1 in the Supporting Information show cross-sectional and top view scanning electron microscope (SEM) images, respectively, of vertically aligned TiO_2 NRs grown on fluorine-doped tin oxide (FTO) slides, before and after decoration (surface modification) with different NP loadings. Figure 1a shows the bare NRs (as grown). The length of the NRs is in average 550–600 nm. It is clear from the SEM images b–d) that when increasing the concentration of the $TiCl_4$ solution from 50 to 200×10^{-3} M, the TiO_2 NP loading consistently increases as well as the average TiO_2 NP size. The TiO_2 NP forms at the NR surface a conformal layer, the thickness

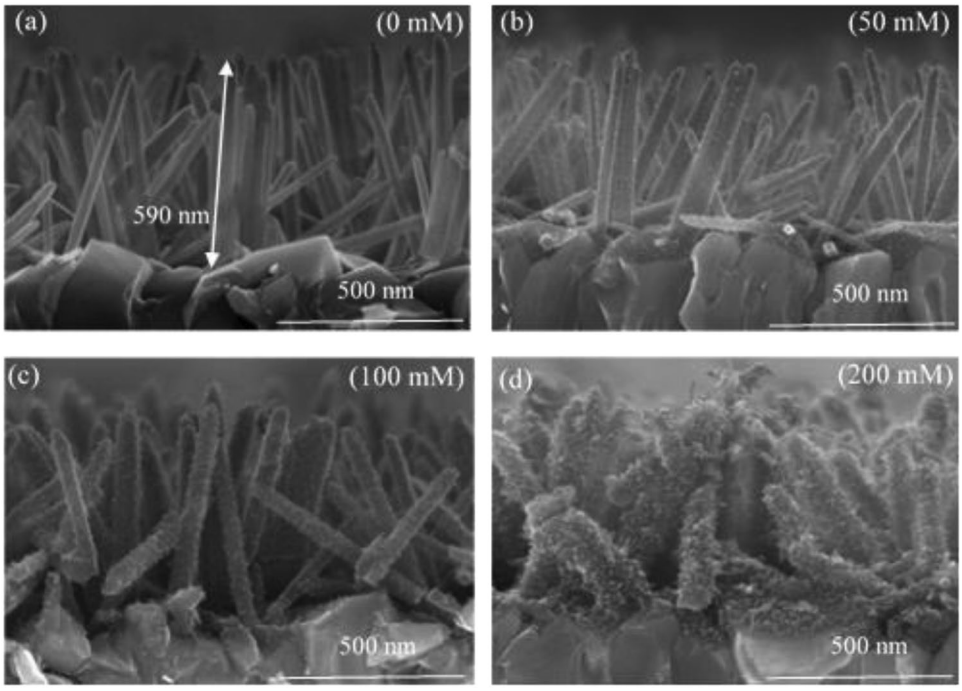

Figure 1. Cross-sectional SEM images of TiO_2 NRs decorated by $TiCl_4$ treatment, using different $TiCl_4$ solution concentrations: a) pristine NRs; b) 50×10^{-3} M; c) 100×10^{-3} M, and d) 200×10^{-3} M.

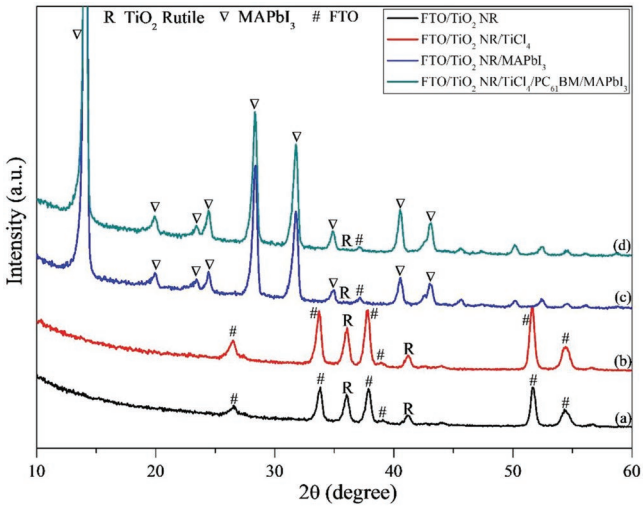

Figure 2. XRD patterns of a) pristine NRs, b) $TiCl_4$-treated NRs, c) NRs/$MAPbI_3$, and d) $TiCl_4$-treated NRs/$PC_{61}BM$/$MAPbI_3$ on FTO.

of which scales with the $TiCl_4$ solution concentration (this is well in line with previous work[25]). The NP seem to form also at the free FTO surface (i.e., FTO surface not coated by NRs).

The X-ray diffraction (XRD) patterns of pure and $TiCl_4$-treated NRs are compiled in **Figure 2**. In general, NRs' features such as diameter, length, and density could be varied by changing growth parameters, such as growth time and temperature, initial reactant concentration, acidity, or additives. Nevertheless, the growth mechanism remains based on the epitaxial relation between the FTO substrate and the growing rutile TiO_2 phase. Precisely, the small lattice mismatch between FTO and rutile TiO_2 phases plays a key role in driving the nucleation and epitaxial growth towards single-crystalline rutile TiO_2 NRs.[26,27]

The XRD data in Figure 2 show that, upon NR growth, peaks appear that agree well with the tetragonal rutile phase. However, compared to common powder diffraction patterns (randomly oriented rutile TiO_2 crystals), the intensity of the (101) diffraction peak (at 36.0°) is relatively high, while, e.g., the peak ascribed to the (110) reflection (at 27.36°, typically a main reflection for a polycrystalline rutile specimen) is absent. This indicates that the NRs are highly oriented with respect to the substrate, supporting the epitaxial growth on FTO. Previous work,[26,27] where similar experimental conditions were used to grow TiO_2 NRs, proved by high-resolution transmission electron microscopy (HR-TEM) analysis the single-crystalline nature of such rutile TiO_2 NRs.

No information on the crystallographic features of the decorated NPs could be obtained by XRD, probably owing to the low loading (below XRD detection limits). However, based on the adopted experimental conditions and previous literature, the deposited NPs are supposed to be composed of anatase phase.[25,28,29]

In the case of dual modification of the ETL, the PSCs were constructed with the following architecture: FTO/TiO_2 NRs/TiO_2 NPs/$PC_{61}BM$/$MAPbI_3$/PDCBT/MoO_x/Ag. An SEM image of the cross-sectional cut of a typical device is provided in **Figure 3**. We also fabricated reference cells either without $PC_{61}BM$ or without $TiCl_4$ treatment.

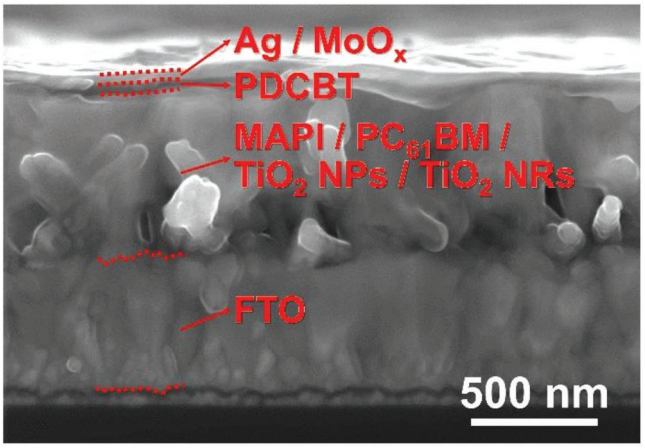

Figure 3. Cross-sectional SEM image of a typical PSC investigated in the present work.

The device performance of the PSCs was assessed by measuring their *J–V* curves under AM 1.5G irradiation (100 mW cm^{-2}); data are compiled in **Figure 4**a. The results for the average photovoltaic parameters of each cell are summarized in **Table 1**. According to the results, the pristine TiO_2 NR-based device shows the lowest performance with a power conversion efficiency (PCE) of 12.2%, a short-circuit current density (J_{SC}) of 21.1 mA cm^{-2}, an open-circuit voltage (V_{OC}) of 0.85 V, and a fill factor (FF) of 69%. The relatively poor performance of this device has to be ascribed to a large density of trap states at the surface of the unmodified TiO_2 NRs.[30]

The $TiCl_4$ and $PC_{61}BM$ treatments are expected to influence the charge extraction across the TiO_2 ETL/perovskite interface. Figure 4a shows the *J–V* curves for devices (champion cells) fabricated by different ETL treatments, while in Figure 4b–e we have compiled a statistical evaluation of the photovoltaic parameters for devices based on differently treated ETLs. The photovoltaic parameters of these cells are also summarized in Table 1.

We first explored the effect of $TiCl_4$ and $PC_{61}BM$ treatments separately. For the devices fabricated from ETLs treated with only $TiCl_4$ (100×10^{-3} M), the cell performance increases in average from 12.2% (reference cell with pristine NRs) to 13.7%. This is caused by a slight increase of the J_{SC} and, more importantly, by a significant improvement of the V_{OC} (from 0.85 V for the reference device to 0.94 V). Here the deposited TiO_2 NP layer plays a key role, i.e., it provides a charge blocking effect by forming a barrier layer at the FTO/perovskite interface,[31] thereby aiding in suppressing detrimental charge recombination. It has been also reported that $TiCl_4$ treatment can also effectively reduce the density of surface defects in metal oxide ETLs.[11,22,25]

To prove the synergistic effects arising from decorating the NRs by the $TiCl_4$ treatment, we fabricated control devices without NRs and by a direct $TiCl_4$ treatment of the FTO substrates. With this treatment, the FTO slides result covered in a homogeneous fashion by TiO_2 NPs, the size of which is in average comparable to that of NPs decorated on the NRs (see the SEM of a typical $TiCl_4$-treated FTO slide in Figure S2 in the Supporting Information). As illustrated in Figure S3 (and Table S1)

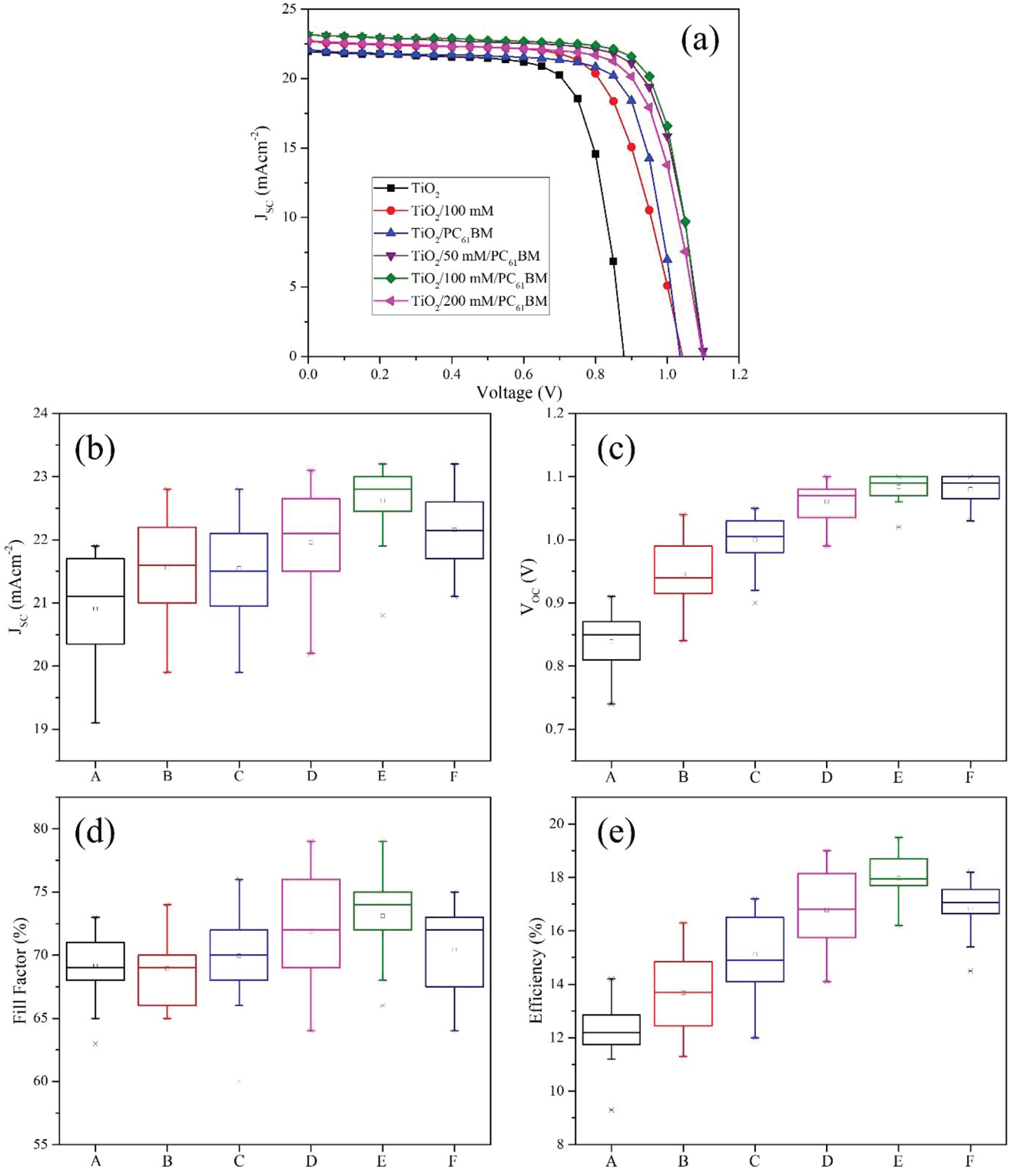

Figure 4. a) Current density–voltage characteristics of the best devices fabricated by different ETL modifications; b–e) statistics of the photovoltaic parameters for devices constructed from A) pristine NRs; B) NRs treated with 100×10^{-3} M $TiCl_4$; C) NR coated with $PC_{61}BM$; D) NR/50×10^{-3} M $TiCl_4/PC_{61}BM$; E) NR/100×10^{-3} M $TiCl_4/PC_{61}BM$; and F) NR/200×10^{-3} M $TiCl_4/PC_{61}BM$.

in the Supporting Information, the devices produced from TiO_2 NP-decorated FTO show a clearly worse performance (PCE of the champion cell: 10.6%) compared to cells fabricated from pristine TiO_2 NRs (14.2%). This confirms not only the benefit of using the NR arrays as nanostructured ETL but also the synergistic effects arising from their surface modification with TiO_2 NPs.

Table 1. Summary of the photovoltaic parameters of devices fabricated from differently treated ETLs.

ETL construction	J_{SC} [mA cm^{-2}]	V_{OC} [V]	FF [%]	PCE_{avg} [%]	PCE_{max} [%]
TiO_2 NRs	21.1±0.83	0.85±0.04	69±2.5	12.2±1.04	14.2
TiO_2 NRs/100×10^{-3} M $TiCl_4$	21.6±0.82	0.94±0.06	69±2.8	13.7±1.4	16.3
TiO_2 NRs/$PC_{61}BM$	21.5±0.83	1±0.04	70±3.9	14.9±1.4	17.2
TiO_2 NRs/50×10^{-3} M $TiCl_4$/$PC_{61}BM$	22.1±0.81	1.07±0.03	72±4.7	16.8±1.5	19
TiO_2 NRs/100×10^{-3} M $TiCl_4$/$PC_{61}BM$	22.8±0.56	1.09±0.02	74±3.4	17.9±0.95	19.5
TiO_2 NRs/200×10^{-3} M $TiCl_4$/$PC_{61}BM$	22.1±0.58	1.09±0.02	72±3.5	17±1.02	18.2

For devices constructed from ETLs treated with $PC_{61}BM$ only, the PCE reached 14.9% and the V_{OC} increased to 1 V. $PC_{61}BM$ binds to the hydroxyl groups at the TiO_2 surface through the carboxylic acid anchoring group, while the fullerene moiety faces the perovskite side. As reported by Wojciechowski et al., the V_{OC} and PCE enhancement can be ascribed to an interfacial alteration of the TiO_2/perovskite junction, i.e., $PC_{61}BM$ passivates or inhibits the formation of trap states at the interface (sub-bandgap states originated by under-coordinated surface Ti(IV) ions), on the TiO_2 surface through the carboxylic acid anchoring group, and on the perovskite side by the fullerene moiety.[32–35] This in turn prevents interfacial electrostatic barriers and provides swift charge (electron) mobility across the ETL/perovskite interface.[33]

It is worth pointing out that for both single modifications (either $TiCl_4$ treatment or $PC_{61}BM$ deposition) the cell performance enhancement should be attributed mainly to an evident increase of the V_{OC}, while the J_{SC} improves only to a minor extent and the FF remains virtually unchanged.

We then investigated the dual modification of TiO_2 NR ETLs, i.e., by $TiCl_4$ treatment combined to a subsequent $PC_{61}BM$ deposition. Upon dual modification, we observed a maximized improvement of the device performance. Such an improvement shows a clear dependence on the $TiCl_4$ concentration and is particularly pronounced when treating the TiO_2 NRs with a 100×10^{-3} M $TiCl_4$ solution. Under optimized conditions, the cells delivered superior photovoltaic parameters with a V_{oc} as high as 1.09 V along with improved J_{sc} of 22.8 mA cm^{-2} and FF of 74%, resulting in an average PCE of 17.9%. The champion device achieved a J_{SC} of 23.2 mA cm^{-2}, a V_{OC} of 1.1 V, an FF of 77%, and a PCE of 19.5%. To the best of our knowledge, this is the highest cell performance reported for TiO_2 rutile NR-based devices fabricated with methylammonium lead triiodide ($MAPbI_3$) light absorber (see Table S2 in the Supporting Information for a summary of the highest cell performance values reported in the literature). Perspective wise, we expect further enhancements in cell efficiency by replacing MAPI with more recently developed and better performing light absorbers, such as mixed cation/anion hybrid perovskite materials.[36]

Aside from the beneficial effect of the $PC_{61}BM$ interlayer and the blocking effect of NPs (outlined above), an additional reason for the performance enhancement can be associated with the more negative conduction band (CB) edge of anatase NPs with respect to the CB minimum of the rutile NRs: as demonstrated by Yang et al.,[31] such energetic situation favors efficient transfer of photo-generated electrons from $MAPbI_3$ to the CB of anatase (NPs) and then onward to the CB of rutile NRs. In addition, the $TiCl_4$ treatment increases the roughness of the NR, providing a nanostructured interfacial contact between the ETL and the perovskite which can thereby sustain a more efficient charge separation and transfer.[37] Nevertheless, a further increase of NPs loading, i.e., a thicker TiO_2 NP layer, was found to cause a decline in cell efficiency (Figure 4 and Table 1). The charge transport across the NP layer may occur via "random walk", through the NP and across the NP boundaries. The thicker the NP layer, the larger the number of diffusion paths from a statistical point of view, and hence the less efficient the charge transport. This decreases the charge carrier collection efficiency,[21,25] as suggested by the dramatic drop of J_{SC} and FF (this aspect is discussed also below along with the results of impedance spectroscopy, IS).

A summary of the effect of the $TiCl_4$ and $PC_{61}BM$ treatments is outlined in Figure 4b–e. The characterization of 20 devices fabricated for each condition proves the consistency of the statistical distribution and tendency of the performance parameters. Overall, one can conclude that each parameter is maximized by combining the $TiCl_4$ and $PC_{61}BM$ treatments, and a most optimized $TiCl_4$ concentration is 100×10^{-3} M.

The V_{OC}, as mentioned above, is significantly affected by the ETL/perovskite interface modification. The average value increases from 0.85 V for the reference device to 1.09 V for the dual modification. This result may be ascribed to the reduction of the electronic disorder at the ETL/perovskite interface.[3] In general, the "electronic disorder" can be interpreted as a measure of the distribution of the electronic density of states (DOS). The electronic states at the ETL/perovskite interface can feature a broad distribution, i.e., can be subject to a large energy disorder originating from structural and chemical inhomogeneity, low crystallinity, random molecular orientation, interactions with neighboring molecules, and presence of impurities, among others. Higher disorder, e.g., in the titania ETL can increase the number of trap sites in the device structure, which eventually leads to electron–hole recombination and short charge carrier lifetimes. Here, the $TiCl_4$ treatment is proven to passivate the titania surfaces, lowering the DOS and reducing the disorder level, which in turn lowers the interfacial charge transfer resistance, enhances the open circuit voltage and thus maximizes the device performance.[3,38]

The increase of current density for devices based on dual modification is supported by a clear enhancement of the device external quantum efficiency (EQE), as shown in **Figure 5**a. The J_{SC} values for the device fabricated from pristine TiO_2 NRs and for the cell produced by dual modification ($TiCl_4$ and $PC_{61}BM$ treatments) are 19.5 and 21.1 mA cm^{-2},

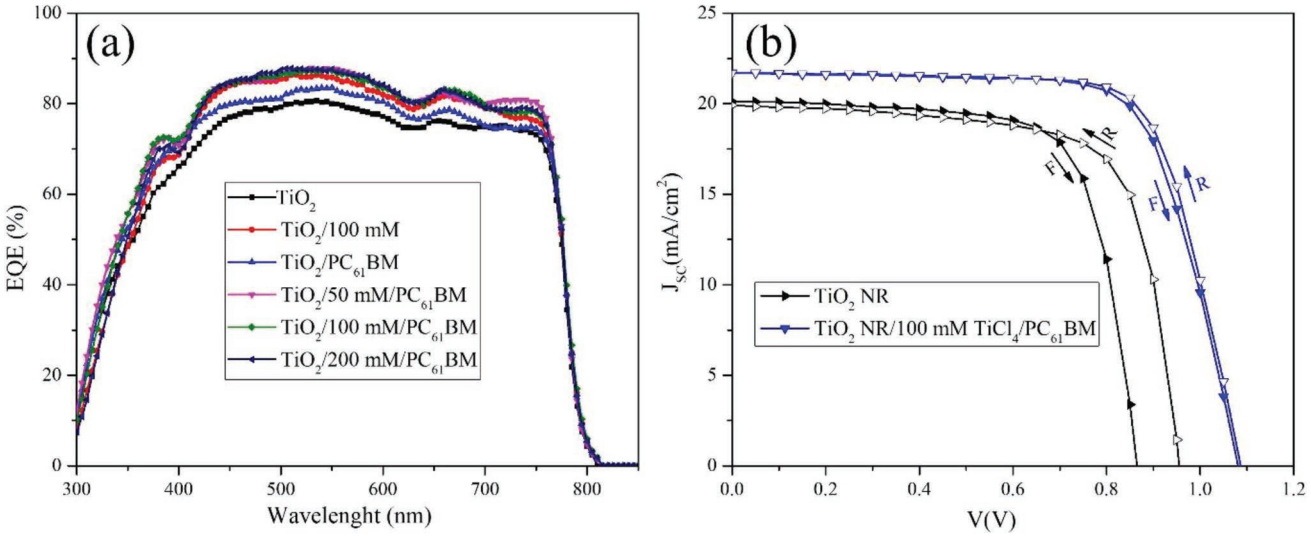

Figure 5. a) EQE spectra of PSCs constructed from differently treated TiO_2 NRs; b) hysteresis curves of perovskite devices based on pristine TiO_2 NRs and TiO_2 NRs modified by an optimized $TiCl_4$ and $PC_{61}BM$ treatment (F and R indicate the forward and reverse scans, respectively).

respectively (these data are consistent with the values derived from the *J–V* curves). Besides, the FF enhancement (from 69% for the reference device to 74% measured by ETL dual modification) can be ascribed to a decrease of the charge transport resistance and to a better filling of the perovskite in the ETL structure.[3]

Figure S4a in the Supporting Information shows the current density delivered by the best performing device: a stable current density of ≈21.8 mA cm^{-2} is tracked under steady-state conditions; this result is in agreement with the *J–V* curves and EQE data. We evaluated the stability for a device fabricated with the following cell architecture: FTO/TiO_2 NRs/(100×10^{-3} M) TiO_2 NPs/$PC_{61}BM$/$MAPbI_3$/PDCBT/MoO_x/Ag. The photovoltaic performance was assessed for the as-fabricated device as well as after storing the device for 7 and 14 d. The results, provided in Figure S4b in the Supporting Information, show that J_{SC} drops to some extent over time, suggesting that the perovskite is undergoing partial degradation as also reported in previous work.[39] On the contrary, the V_{OC} remains almost unaltered. In this context, we anticipate the use of more stable mixed cation/anion perovskite materials[10] to reduce efficiency losses ascribed to perovskite decomposition.

Figure 5b shows the effect of the combined $TiCl_4$ treatment and $PC_{61}BM$ modification on cell hysteresis with respect to a reference device (constructed from pristine NRs). Severe loss in cell performance were measured by sequential forward and reverse bias scans for the device fabricated with unmodified NRs, while the hysteresis is considerably suppressed for the device modified with both $TiCl_4$ and $PC_{61}BM$. The influence of the interface engineering on the open-circuit voltage is evident: for pristine NR, there is a considerable difference between the V_{OC} measured in forward and reverse scans, while after the dual surface modification the difference becomes negligible. Previous work demonstrated that trap states at the TiO_2 ETL surface (i.e., at the ETL/perovskite interface) are the major cause for hysteresis.[33,40,41] Our results suggest that the dual ETL modification leads to an effective passivation of such trap states, thereby improving the charge mobility across the ETL/perovskite interface.

UV–vis diffuse reflectance and steady-state photoluminescence (PL) measurements were conducted to further study the light absorbance feature and charge transfer properties of the perovskite/ETL architectures based on various surface engineering methods. The data are compiled in **Figure 6** (the optical features of differently treated ETLs are reported as reference data in Figure S5 in the Supporting Information). The UV–vis spectra (Figure 6a) show a higher absorbance for the perovskite deposited on ETLs modified by $TiCl_4$ and $PC_{61}BM$ treatments, particularly for NRs treated under optimized conditions (100×10^{-3} M $TiCl_4$ solution). This can be ascribed to enhanced internal light scattering effects induced by the NR surface roughness, which seems to increase the overall photon harvesting by the perovskite. At the same time, the SEM images in Figure S6 in the Supporting Information and the grain size distribution statistics shown in Figure S7 in the Supporting Information confirm that the optical properties of devices fabricated from differently treated ETLs cannot be ascribed to the perovskite crystallographic features. The grain size statistics of $MAPbI_3$ layers grown on NRs appears in fact not to be affected by different ETL surface treatments. Moreover, the XRD patterns in Figure 2 reveal that the crystallographic properties of the perovskite grown on unmodified and modified ETLs do not feature remarkable differences.

The PL spectra of perovskite layers formed on differently treated ETLs are compiled in Figure 6b. Steady-state PL can provide a measure of the quality of the perovskite film (e.g., to assess the effects of defect passivation) or of the quenching efficiency (e.g., by charge extraction). The results point to a more efficient charge extraction for the modified ETL/perovskite interface compared to perovskite layers grown on pristine (unmodified) NRs. The highest PL (i.e., worst quenching yield) is measured for the perovskite layer grown on pristine NRs. After $TiCl_4$ or $PC_{61}BM$ modification of the ETL, the PL intensity substantially decreased. Precisely, the most effective

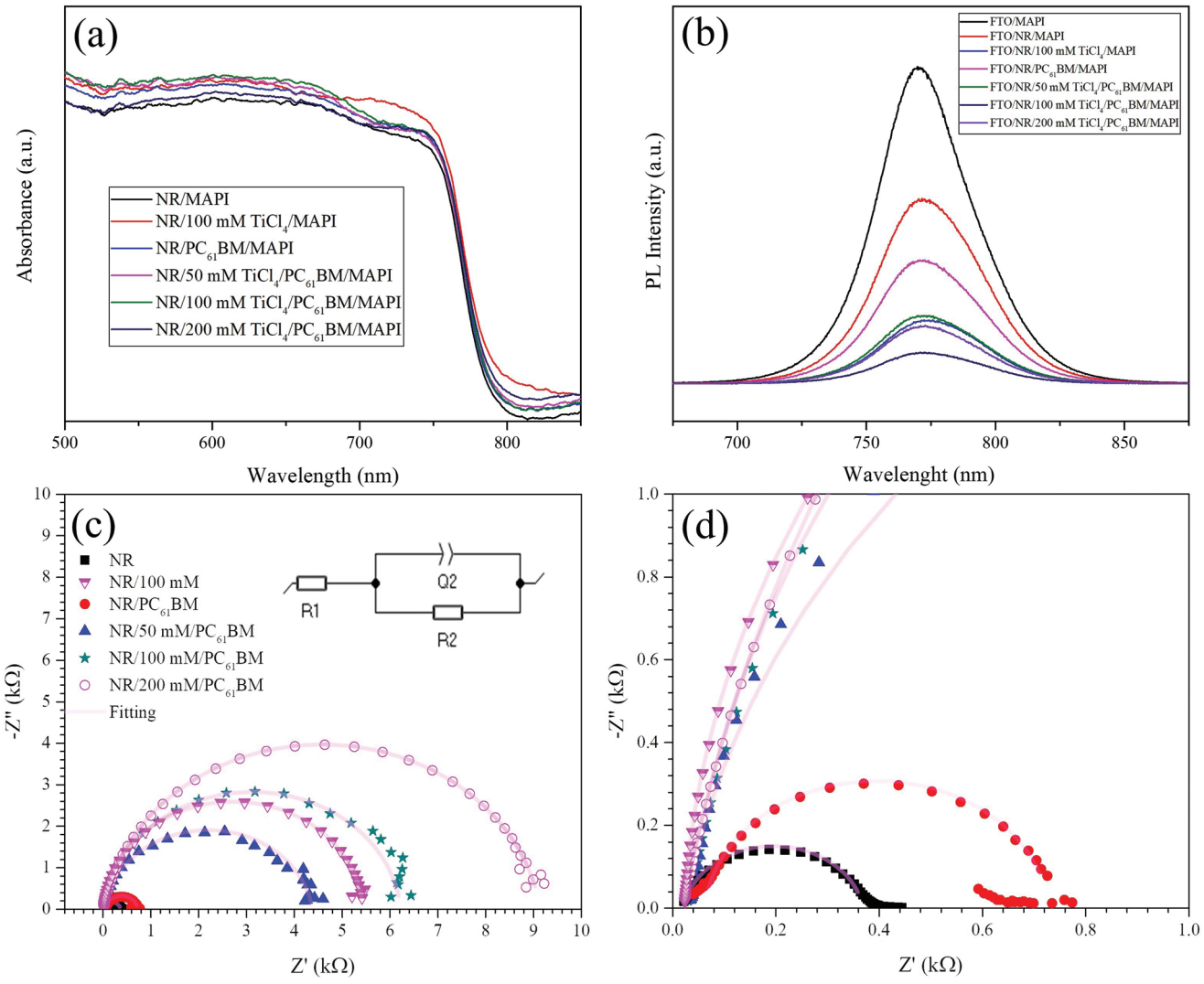

Figure 6. a) Visible light absorption and b) PL spectra of $MAPbI_3$ layers grown on differently treated TiO_2 NRs; c,d) Results of impedance spectroscopy: c) Nyquist plots measured under light illumination with an applied voltage of 0.8 V along with the relative equivalents circuit used for fitting; and d) enlarged view of data in (c).

PL quenching is reached by a $TiCl_4$ treatment with $TiCl_4$ concentration of 100×10^{-3} M combined with $PC_{61}BM$ modification; the results are well in line with the data discussed above and further prove that TiO_2 NRs modified by a combined $TiCl_4$ and $PC_{61}BM$ treatment can lead to a most efficient extraction of photo-excited electrons from the light absorber.[41]

Solid-state IS was performed to determine the charge recombination properties of reference, $PC_{61}BM$- and/or $TiCl_4$-treated devices.[42] The results are reported in Figure 6. The IS measurements were carried out under light illumination, in a high-frequency range (1 MHz to 1 Hz), and at an applied bias of 0.8 V. The semicircle in the Nyquist plots (see in Figure 6c a magnified view of the spectra of different devices) is assigned to the parallel combination of the recombination resistance and the geometric capacitance of the devices. For data analysis, a constant phase element (*Q*) instead of an ideal super-capacitor element was used, in order to improve the quality of the fitting. The equivalent electric parameters were extracted accordingly and are compiled in Table S3 in the Supporting Information. From a diagnostic point of view, in previous work, it has been reported that a high recombination resistance (i.e., low recombination of generated charges) results typically in highly efficient PSCs.[10] In line with the photovoltaic parameters, we observed high recombination resistance for cells fabricated from ETLs modified by dual $TiCl_4$ and $PC_{61}BM$ treatment. This once again confirms the positive effects of the dual surface treatment in suppressing detrimental charge recombination phenomena. According to the impedance results, the TiO_2 NPs (formed by $TiCl_4$ treatment) seem to have a considerable effect in decreasing the charge recombination rate. This is more likely caused by the TiO_2 NP blocking layer formed at the free FTO surface, which prevents leakage current that could originate from a direct perovskite/FTO contact. Here, we should mention that the growth of TiO_2 NRs can be ascribed to heterogeneous nucleation (of TiO_2 seeds on the FTO substrate) driven by lower degrees of super-saturation.[27] The NR coverage (or NR density

at the FTO surface) can be determined by the competition between seed nucleation and NR growth rates, which in turn is affected by the experimental conditions (e.g., Ti precursor and HCl concentrations). The experimental conditions here adopted lead to rutile TiO_2 NRs with an open structure, i.e., the NR density leaves empty space for the perovskite filling. While this on the one side is beneficial for an effective infiltration and crystallization of the perovskite within the ETL, the free FTO surface left behind negatively affects the cell functionality (perovskite/FTO contact) and has therefore to be coated (blocking layer) via an optimized $TiCl_4$ treatment. Besides, by increasing the concentration of the $TiCl_4$ solution, the modified ETLs show a gradually higher charge recombination resistance. This indicates that the $TiCl_4$ modification is beneficial as it forms at the NR surface a TiO_2 NP buffer interface that enhances the charge transfer.

3. Conclusion

We systematically explored the effects of multiple ETL surface treatments on the efficiency of $MAPbI_3$ PSCs. Our results showed that also in the case of mesoporous nanostructured ETLs the open-circuit voltage, and therefore the overall cell efficiency, can be largely improved by an adequate engineering of the interface between the ETL and the perovskite absorber. We observed that a combined $TiCl_4$ and $PC_{61}BM$ treatment is a pre-requisite to fabricate efficient PSCs from ETLs consisting of arrays of single crystalline TiO_2 NRs. The dual treatment led to a champion efficiency of 19.5% and enabled a nearly complete suppression of the device hysteresis. The performance enhancement originates from a more efficient charge transfer across the ETL/perovskite interface, which is caused by the passivation of defects and trap states at the TiO_2 ETL surface. This ETL surface engineering approach can potentially provide a further cell performance enhancement if combined to better performing, mixed cation/anion hybrid perovskite materials.

4. Experimental Section

Preparation of Rutile TiO_2 Nanorod ETL: Laser patterned FTO substrates (7 Ω m^{-2}, Solaronix) were cleaned by ultrasonication in acetone first, then in isopropanol, and were then dried in a stream of nitrogen. TiO_2 NRs were grown directly on the FTO surfaces by a hydrothermal process.[43] Typically, 1 mL of titanium isopropoxide (Sigma–Aldrich) was added to an equal volume (50 mL: 50 mL) of a mixture of DI water and HCl (37%, Sigma–Aldrich) in a 250 mL Teflon-lined autoclave. This mixture was stirred for 15 min. Then, the pre-cleaned FTO was immersed in the solution facing down. The hydrothermal synthesis was performed at 180°C for 2.5 h. Finally, the as-prepared NRs were annealed at 450 °C for 1 h in air furnace. For the $TiCl_4$ treatment, experimental conditions reported elsewhere were adopted.[44] briefly, the TiO_2 NRs were immersed in aqueous $TiCl_4$ solutions of different concentrations (50, 100, and 200 × 10^{-3} M) at 70 °C for 30 min. The samples were then heat-treated at 450 °C for 10 min to crystallize the deposited NPs into anatase phase.

Device Fabrication: The as-prepared FTO supported NR layers (ETL) were moved to a nitrogen-filled glovebox and processed as substrates to fabricate the PSCs. $PC_{61}BM$ (99.5%, Solenne) solution (10 mg mL^{-1} in chlorobenzene, Sigma–Aldrich) was spin-coated on the substrate followed by heating at 110 °C for 5 min. For the preparation of the perovskite solution, 710 mg of PbI_2 (Lumtec) and 240 mg of CH_3NH_3I (Lumtec) were dissolved in a mixture of DMF (dimethylformamide; Sigma–Aldrich) and DMSO (dimethyl sulfoxide; Sigma–Aldrich) at 40 °C. The perovskite precursor was deposited on the $PC_{61}BM$ layer by spin-coating at a speed of 4000 rpm for 15 s followed by blowing off the leftover solvent with a N_2 stream. The samples were then annealed on a hot plate at 110 °C for 10 min. The hole transport material solution, consisting of a 10 mg mL^{-1} solution of poly[5,5′-bis(2-butyloctyl)-(2,2′-bithiophene)-4,4′-dicarboxylate-alt-5,5′-2,2′-bithiophene] (PDCBT, 1-Material) in chlorobenzene, was spin-coated on the perovskite layer at 2000 rpm for 30 s and annealed at 70 °C for 3 min. Finally, a 15-nm-thick MoO_x (Alfa Aesar) and 120-nm-thick Ag films were evaporated on PDCBT by using a thermal evaporation system. A mask was used to pattern the deposited MoO_x and Ag films.

Characterization: Current density–voltage (*J–V*) and steady-state current density (J_{MPP}) characterization of the devices was carried out under simulated solar light illumination (AM1.5G) with a light intensity of 100 mW cm^{-2} (calibrated with a Si-cell). The EQE spectra were recorded using an Enli Technology (Taiwan) EQE measurement system (QE-R). Prior to measurement, the light intensity at each wavelength was calibrated by using a standard single-crystal Si photovoltaic cell.

The morphology and crystalline structure of the nanostructured TiO_2 ETLs and perovskite layers were characterized by a field-emission SEM (Fe-SEM, S4800, Hitachi) and by XRD (X'pert Philips MPD diffractometer, using a Panalytical X'celerator detector and graphite monochromized Cu Kα radiation, λ = 1.54056 A Å) respectively. The perovskite grain size distribution was determined by using the software Image J.

UV–vis light absorption spectra were recorded using an Avantes spectroscopy system (AvaLight-DH-S-BAL Balanced Power and AvaSpec-ULS2048L StarLine Versatile Fiber-optic Spectrometer) equipped with an integrating sphere (a $BaSO_4$ standard white board was used as reference).

Solid-state IS measurements were carried out under 0.1 sun illumination, at 0.8V and in a frequency range from 1 MHz to 1 Hz, by using of an Agilent HP 4192A impedance analyzer. Steady-state PL was measured using an Argon-ion 488-nm laser excitation source, a Horiba monochromator, and a Silicone detector.

Supporting Information

Supporting Information is available from the Wiley Online Library or from the author.

Acknowledgements

The authors would like to acknowledge the ERC, the DFG, and the DFG cluster of excellence "Engineering of Advanced Materials" for financial support. Gihoon Cha (Department of Materials Science and Engineering WW4-LKO, University of Erlangen-Nuremberg, Germany) and Dr. Nhat Truong Nguyen (current affiliation: GAO Materials Chemistry Research Group, Department of Chemistry, University of Toronto, Canada) are acknowledged for their help with XRD and optical measurements, respectively. N.L. gratefully acknowledges the financial support from the DFG research grant: BR 4031/13-1. C.J.B. gratefully acknowledges the financial support through the "Aufbruch Bayern" initiative of the state of Bavaria (EnCN and SFF), the Bavarian Initiative "Solar Technologies go Hybrid" (SolTech), and the projects SFB 953 (DFG, project no. 182849149) and DFG INST 90/917-1 FUGG.

Conflict of Interest

The authors declare no conflict of interest.

Keywords

defect passivation, $PC_{61}BM$, perovskite solar cells, $TiCl_4$, TiO_2 nanorods

Received: November 21, 2019
Revised: December 18, 2019
Published online: January 9, 2020

[1] C. Chen, Y. Cheng, Q. Dai, H. Song, *Sci. Rep.* **2016**, *5*, 17684.
[2] N. J. Jeon, J. H. Noh, W. S. Yang, Y. C. Kim, S. Ryu, J. Seo, S. Il Seok, *Nature* **2015**, *517*, 476.
[3] M. Abdi-Jalebi, M. I. Dar, A. Sadhanala, S. P. Senanayak, F. Giordano, S. M. Zakeeruddin, M. Grätzel, R. H. Friend, *J. Phys. Chem. Lett.* **2016**, *7*, 3264.
[4] J. Min, Z. Zhang, Y. Hou, C. O. Ramirez Quiroz, T. Przybilla, C. Bronnbauer, F. Guo, K. Forberich, H. Azimi, T. Ameri, E. Spiecker, Y. Li, C. J. Brabec, *Chem. Mater.* **2015**, *27*, 227.
[5] F. Guo, H. Azimi, Y. Hou, T. Przybilla, M. Hu, C. Bronnbauer, S. Langner, E. Spiecker, K. Forberich, C. J. Brabec, *Nanoscale* **2015**, *7*, 1642.
[6] S. Ameen, M. Nazim, M. S. Akhtar, M. K. Nazeeruddin, H. Shin, *Nanoscale* **2017**, *9*, 17544.
[7] Y. Hou, W. Chen, D. Baran, T. Stubhan, N. A. Luechinger, B. Hartmeier, M. Richter, J. Min, S. Chen, C. O. R. Quiroz, N. Li, H. Zhang, T. Heumueller, G. J. Matt, A. Osvet, K. Forberich, Z. Zhang, Y. Li, B. Winter, P. Schweizer, E. Spiecker, C. J. Brabec, *Adv. Mater.* **2016**, *28*, 5112.
[8] S. Wu, C. Chen, J. Wang, J. Xiao, T. Peng, *ACS Appl. Energy Mater.* **2018**, *1*, 1649.
[9] W. Wu, L. Wang, *Adv. Funct. Mater.* **2018**, *28*, 1804356.
[10] L. Yang, X. Wang, X. Mai, T. Wang, C. Wang, X. Li, V. Murugadoss, Q. Shao, S. Angaiah, Z. Guo, *J. Colloid Interface Sci.* **2019**, *534*, 459.
[11] J. Ma, J. Chang, Z. Lin, X. Guo, L. Zhou, Z. Liu, H. Xi, D. Chen, C. Zhang, Y. Hao, *J. Phys. Chem. C* **2018**, *122*, 1044.
[12] H.-S. Kim, J.-W. Lee, N. Yantara, P. P. Boix, S. A. Kulkarni, S. Mhaisalkar, M. Grätzel, N.-G. Park, *Nano Lett.* **2013**, *13*, 2412.
[13] H. Sun, K. Deng, Y. Zhu, M. Liao, J. Xiong, Y. Li, L. Li, *Adv. Mater.* **2018**, *30*, 1801935.
[14] Z. Lan, X. Xu, X. Zhang, J. Tang, L. Zhang, X. He, J. Wu, *J. Mater. Chem. C* **2018**, *6*, 334.
[15] R. Salazar, M. Altomare, K. Lee, J. Tripathy, R. Kirchgeorg, N. T. Nguyen, M. Mokhtar, A. Alshehri, S. A. Al-Thabaiti, P. Schmuki, *ChemElectroChem* **2015**, *2*, 824.
[16] X. Gao, J. Li, J. Baker, Y. Hou, D. Guan, J. Chen, C. Yuan, *Chem. Commun.* **2014**, *50*, 6368.
[17] A. Nawaz, K. K. Wong, C. Ebenhoch, E. Zimmermann, Z. Zheng, M. N. Akram, J. Kalb, K. Wang, A. Fakharuddin, L. Schmidt-Mende, *Sol. Energy* **2018**, *170*, 541.
[18] P. Qin, M. Paulose, M. I. Dar, T. Moehl, N. Arora, P. Gao, O. K. Varghese, M. Grätzel, M. K. Nazeeruddin, *Small* **2015**, *11*, 5533.
[19] G. Choe, J. Kang, I. Ryu, S. W. Song, H. M. Kim, S. Yim, *Sol. Energy* **2017**, *155*, 1148.
[20] L. Cojocaru, S. Uchida, Y. Sanehira, J. Nakazaki, T. Kubo, H. Segawa, *Chem. Lett.* **2015**, *44*, 674.
[21] A. Yella, L. Heiniger, P. Gao, M. K. Nazeeruddin, M. Grätzel, *Nano Lett.* **2014**, *14*, 2591.
[22] Z. Liu, Q. Chen, Z. Hong, H. Zhou, X. Xu, N. De Marco, P. Sun, Z. Zhao, Y. Cheng, Y. Yang, *ACS Appl. Mater. Interfaces* **2016**, *8*, 11076.
[23] Z. Zhou, S. Pang, Z. Liu, H. Xu, G. Cui, *J. Mater. Chem. A* **2015**, *3*, 19205.
[24] J. Kim, G. Kim, T. K. Kim, S. Kwon, H. Back, J. Lee, S. H. Lee, H. Kang, K. Lee, *J. Mater. Chem. A* **2014**, *2*, 17291.
[25] H. K. Adli, T. Harada, S. Nakanishi, S. Ikeda, *Phys. Chem. Chem. Phys.* **2017**, *19*, 26898.
[26] B. Liu, E. S. Aydil, *J. Am. Chem. Soc.* **2009**, *131*, 3985.
[27] E. Hosono, S. Fujihara, K. Kakiuchi, H. Imai, *J. Am. Chem. Soc.* **2004**, *126*, 7790.
[28] N. T. Nguyen, S. Ozkan, I. Hwang, A. Mazare, P. Schmuki, *Nanoscale* **2016**, *8*, 16868.
[29] S. Feng, A. Runa, L. Liu, J. Wang, P. Su, T. Liu, S. Su, G. Zhu, W. Fu, H. Yang, *J. Mater. Sci. Mater. Electron.* **2018**, *29*, 16903.
[30] C. Liu, R. Zhu, A. Ng, Z. Ren, S. H. Cheung, L. Du, S. K. So, J. A. Zapien, A. B. Djurišić, D. Lee Phillips, C. Surya, *J. Mater. Chem. A* **2017**, *5*, 15970.
[31] J. Yang, W. Liao, J. Wu, *ACS Appl. Mater. Interfaces* **2013**, *5*, 7425.
[32] F. Cai, J. Cai, L. Yang, W. Li, R. S. Gurney, H. Yi, A. Iraqi, D. Liu, T. Wang, *Nano Energy* **2018**, *45*, 28.
[33] K. Wojciechowski, S. D. Stranks, A. Abate, G. Sadoughi, A. Sadhanala, N. Kopidakis, G. Rumbles, C. Li, R. H. Friend, A. K.-Y. Jen, H. J. Snaith, *ACS Nano* **2014**, *8*, 12701.
[34] C. Tao, S. Neutzner, L. Colella, S. Marras, A. R. Srimath Kandada, M. Gandini, M. De Bastiani, G. Pace, L. Manna, M. Caironi, C. Bertarelli, A. Petrozza, *Energy Environ. Sci.* **2015**, *8*, 2365.
[35] Q. Wang, Y. Shao, Q. Dong, Z. Xiao, Y. Yuan, J. Huang, *Energy Environ. Sci.* **2014**, *7*, 2359.
[36] B. Cao, H. Liu, L. Yang, X. Li, H. Liu, P. Dong, X. Mai, C. Hou, N. Wang, J. Zhang, J. Fan, Q. Gao, Z. Guo, *ACS Appl. Mater. Interfaces* **2019**, *11*, 33770.
[37] Y. Zhao, A. M. Nardes, K. Zhu, *Faraday Discuss.* **2014**, *176*, 301.
[38] Y. Shao, Y. Yuan, J. Huang, *Nat. Energy* **2016**, *1*, 15001.
[39] X. Li, S.-M. Dai, P. Zhu, L.-L. Deng, S.-Y. Xie, Q. Cui, H. Chen, N. Wang, H. Lin, *ACS Appl. Mater. Interfaces* **2016**, *8*, 21358.
[40] B. Chen, M. Yang, X. Zheng, C. Wu, W. Li, Y. Yan, J. Bisquert, G. Garcia-Belmonte, K. Zhu, S. Priya, *J. Phys. Chem. Lett.* **2015**, *6*, 4693.
[41] W. Zhou, J. Zhen, Q. Liu, Z. Fang, D. Li, P. Zhou, T. Chen, S. Yang, *J. Mater. Chem. A* **2017**, *5*, 1724.
[42] H. Kim, I. Mora-Sero, V. Gonzalez-Pedro, F. Fabregat-Santiago, E. J. Juarez-Perez, N. Park, J. Bisquert, *Nat. Commun.* **2013**, *4*, 2242.
[43] F. Gao, H. Dai, H. Pan, Y. Chen, J. Wang, Z. Chen, *J. Colloid Interface Sci.* **2018**, *513*, 693.
[44] P. Roy, D. Kim, I. Paramasivam, P. Schmuki, *Electrochem. Commun.* **2009**, *11*, 1001.